

Neutrino Emission from Gamma-ray Burst Jet Propagating inside the Cavity within Active Galactic Nucleus Accretion Disks

HAO-YU YUAN ,¹ WEN-LONG XU,¹ KAI WANG ,¹ AND WEI-HUA LEI ,¹

¹*Department of Astronomy, School of Physics, Huazhong University of Science and Technology, Luoyu Road 1037, Wuhan, 430074, China*

ABSTRACT

Short gamma-ray bursts (sGRBs) from the merger of binary compact objects (BCOs) could occur in the accretion disks of the active galactic nucleus (AGN). Before merging, the BCO will inevitably form a low-density cavity. The sGRB jet will interact with the AGN disk photons during its propagation through the cavity, leading to unique electromagnetic and neutrino signatures. In this work, we investigate the influence of the AGN disk photon field on neutrino emission within the internal dissipation regions of a two-component sGRB jet (a narrow core and a wide wing). We find that, due to the strong AGN disk photon field, the neutrino flux at high-energy part (e.g., PeV to EeV) will be suppressed, while the relatively lower-energy part (e.g., TeV to PeV) will be enhanced. Such a conclusion can enhance the constraints on GRB parameters (e.g., baryonic loading factor and bulk Lorentz factor) based on the future detection or non-detection of high-energy neutrinos from GRBs. Besides, the two-component jet can display two-bump structure at higher and lower energy in the neutrino spectrum. Therefore, the joint observations of electromagnetic and neutrinos emission can help us identify the sGRB jet and its structure in the AGN disk.

Keywords: Neutrino astronomy (1100), Gamma-ray bursts (629), Galaxy accretion disks (562)

1. INTRODUCTION

Active galactic nuclei (AGN) are extremely luminous regions located at the cores of galaxies, fueled by the release of gravitational energy when dense matter accumulates around a central supermassive black hole (SMBH, Lynden-Bell 1969; Shakura & Sunyaev 1973). Searches for electromagnetic counterparts (EM) to binary black hole (BBH) mergers, e.g., the gravitational wave (GW) event GW190521 and the potential EM counterpart ZTF19abanrhr (Abbott et al. 2020; Graham et al. 2020), indicate that AGN disks are likely to host compact binary objects (Graham et al. 2023). Joint observations of GW170817, GRB 170817A, and AT2017gfo reveal that

a binary neutron star (BNS) merger can produce a GW burst, a short gamma-ray burst (SGRB) and kilonova (Abbott et al. 2017; Goldstein et al. 2017; Savchenko et al. 2017; Zhang et al. 2018; Kimura et al. 2021). The multi-messenger properties of BNS mergers in AGN disk are of great interest.

In particular, high-energy neutrinos, which benefit from the negligible absorption, can serve as a unique messenger to probe the activities occurring within the AGN disk. The bursts within the AGN disk can be natural "hidden" cosmic-ray accelerators (Murase et al. 2016; Ma et al. 2025). The interaction between the jet and AGN disk can create several shocks, i.e., the forward shock, reverse shock and collimation shock. Zhou & Wang (2023) found that the forward shock can not efficiently accelerate protons. The higher energy neutrinos (\gtrsim PeV) are contributed by reverse and collimation shocks, but the lower energy neutrinos are only from

Corresponding author: Kai Wang
 kaiwang@hust.edu.cn

leiwh@hust.edu.cn

the reverse shock. Zhu et al. (2021b) found that the choked GRB jet in the AGN disk can produce TeV-PeV neutrinos through the reacting between the protons and jet head photons, and the neutrinos emission may be detected by IceCube. The evolution of the binary compact object (BCO) can throw strong winds (Kimura et al. 2021). On the one hand, the interaction between the wind and AGN disk can produce the neutrino emission (Ma & Wang 2024; Zhou et al. 2023; Zhu et al. 2021a), on the other hand, the wind can blow away the AGN disk gas around the BCO, forming a low-density cavity, and the GRB jet will not be choked (Kimura et al. 2021; Yuan et al. 2022; Yuan & Lei 2025).

Although the successful jet can be observed when the cavity is formed, the EM emission of the jet would be affected by AGN disk photon fields, especially GeV emission (Yuan et al. 2022). In addition, the AGN disk photon fields can also mediate proton acceleration and cooling. Yuan et al. (2022) discuss qualitatively that the AGN disk photon field can influence the efficiency of neutrino emission, but they do not perform a detailed analysis of the radiation properties of neutrinos. The emission of neutrinos at different energy range influenced by the photon field of AGN disks is a factor that has not been addressed in current research.

Additionally, neutrino energy and fluence also depend on the jet Lorentz factor and isotropic luminosity (Kimura et al. 2017). Therefore, jet internal energy distributions and Lorentz factor profiles shape neutrino emission, which requires structured jets rather than uniform top-hat models. Observations and simulations confirm that GRB jets are structured (Zhang et al. 2004; Dai & Gou 2001). We implement a two-component system—a fast narrow core and a slow wide sheath—successfully applied to some GRBs, e.g., GRB 051221A (Jin et al. 2007) and the “brightest of all time” burst, GRB 221009A (Zheng et al. 2024).

In this work, we include the cavity created before jet launch and focus on the impact of the AGN disk photon field on neutrino radiation within the internal dissipation region of the sGRB jet. Besides, we consider the jet has two components, which are perpendicular to the AGN disk mid-plane, and the line of sight is on-axis. The paper is organized as follows. In Section 2, we introduce the model framework and ingredients; The results of the numerical calculation are displayed in Section 3. Conclusions and discussions are drawn in Sec-

tion 4. Throughout the paper, primed quantities denote those in the jet comoving frame, and unprimed quantities refer to the observer frame.

2. MODEL OVERVIEW

A cavity would be created in AGN disks prior to the BCO (e.g., BNS and NS-BH) merger, allowing the jet to be unaffected by the AGN disk material (Kimura et al. 2021). When the jet traverses the cavity, the electron energy spectra and electromagnetic radiation characteristics will be altered by the EIC process involving AGN disk photon fields and the jet’s electrons (Yuan et al. 2022). We incorporate both pre- and post-EIC scattering contributions of AGN disk photon fields to neutrino radiation. In addition, we consider the jet has two components (a fast narrow core and a slow wide wing), perpendicular to the AGN disk plane, with the line of sight aligned along the jet’s axis. The schematic picture for our model is displayed in Fig. 1.

In the research, we consider two distinct AGN disk models (see Sec.2.1) to examine their effects on the results. Our investigation focuses on jet dissipation processes at dissipation radius (r_{diss}), including internal shocks (Rees & Meszaros 1994) and magnetic reconnection (McKinney & Uzdensky 2012). The emission of the internal dissipation can be described by Band component (Band et al. 1993). The presence of the synchrotron radiation death line implies that synchrotron emission can not fully explain the Band component in the GRB prompt emission (Preece et al. 1998; Mészáros & Rees 2000; Zhang 2018). Therefore, we adopt the empirical Band function to describe the photon number spectrum of the jet emission in the internal dissipation region, which can be expressed as (Band et al. 1993),

$$n'_{\text{band}}(\varepsilon'_{\gamma}) \propto \begin{cases} \varepsilon'^{\alpha}_{\gamma} \exp\left(-\frac{\varepsilon'_{\gamma}}{\varepsilon'_{\gamma,0}}\right), & \varepsilon'_{\gamma} < (\alpha - \beta)\varepsilon'_{\gamma,0} \\ \left[(\alpha - \beta)\varepsilon'_{\gamma,0}\right]^{\alpha - \beta} \times \\ \exp(\beta - \alpha)\varepsilon'^{\beta}_{\gamma}, & \varepsilon'_{\gamma} > (\alpha - \beta)\varepsilon'_{\gamma,0} \end{cases}, \quad (1)$$

where $\varepsilon'_{\gamma,0} = \varepsilon'_{\gamma,p}/(2 + \alpha)$ is the break energy and $\varepsilon'_{\gamma,p}$ is the peak energy of the spectrum. α and β are the low and high energy photon spectral indices, e.g., $\alpha = -1$ and $\beta = -2$ (Preece et al. 2000). The normalization factor of Eq.1 can be obtained by $\epsilon_e L_{j,\text{iso}}/4\pi c \Gamma_j^2 r_{\text{diss}}^2 =$

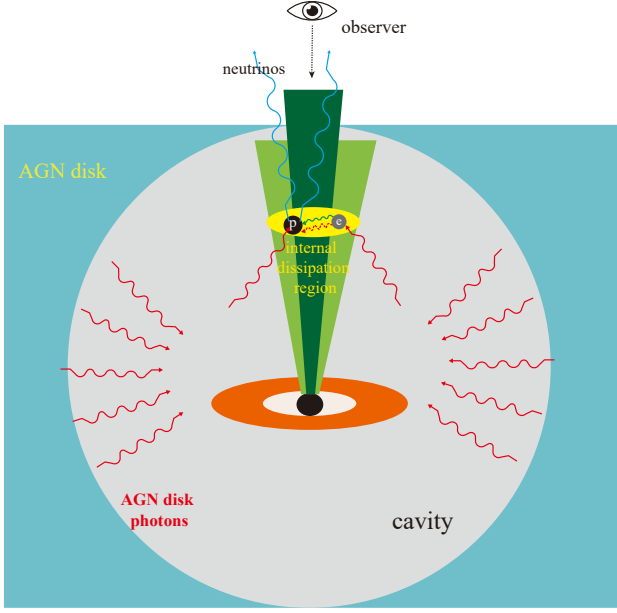


Figure 1. A schematic picture of the jet launched by the BCO merger embedded in the AGN disk. The cavity will be created by the powerful outflow during the BCO evolution. The area of the AGN disk and the cavity are presented by the light blue and the light gray shadows, respectively. The sGRB jet contains two components, a narrow core (dark green cone) and a wide wing (light green cone). The red rays represent the AGN disk photons, which can enter the jet and affect the cooling of protons and electrons. The yellow area is the internal dissipation region of the jet. The AGN disk photons (red solid rays) may undergo two distinct experiences: one is directly reacting with protons (dark filled circle), and the other is being scattered by electrons (grey filled circle) and then reacting with protons. The red dashed ray represents the scattered AGN disk photons, and the green ray is the photons from electron cooling processes, e.g., synchrotron emissions and synchrotron self-Compton. The blue rays are the neutrino emission from the $p\gamma$ reactions.

$\int_{\varepsilon'_{\gamma,m}}^{\varepsilon'_{\gamma,M}} d\varepsilon'_{\gamma} \varepsilon'_{\gamma} n'_{\text{band}}(\varepsilon'_{\gamma})$, where ϵ_e is the fraction of jet kinetic energy that is converted to electrons, $L_{j,\text{iso}}$ is the isotropic kinetic luminosity of the jet, Γ_j is the jet bulk Lorentz factor, $\varepsilon'_{\gamma,m}$ and $\varepsilon'_{\gamma,M}$ are the minimum and maximum photon energy. Besides, we derive the Comptonized disk photon spectrum in Sec. 2.2. Using the photon spectrum in the dissipation region and a given proton spectrum, the neutrino radiation fluence can be obtained (see Sec. 2.3).

2.1. AGN disk and disk radiation field

In the research, we adopt two different AGN disk models, i.e., Sirko & Goodman (2003) and Thompson et al.

(2005), which are respectively referred to as SG03 and TQM05 models. Both models extend inner thin accretion disks to larger radii, explaining AGN luminosity, but require extra pressure against outer collapse, which is inevitable in the α -disk of Shakura & Sunyaev (1973). The SG03 model suggests that radiation pressure, such as that from star fusion, counteracts collapse in the outer area, which sustaining constant accretion rate across the disk. The TQM05 model replaces local viscous stress with non-local torque for mass advection, adding star formation effects on the radial accretion profile.

We use the method developed by Gangardt et al. (2024) to calculate the radial profile of the AGN disk for SG03 and TQM05 models, e.g., the effective temperature $T_{d,\text{eff}}$ and the half-thickness H . We adopt three different masses for the central SMBH, $M_{\bullet} = 10^6 M_{\odot}$, $10^7 M_{\odot}$, and $10^8 M_{\odot}$, and the results are shown in Fig. 2.

Similar to Yuan et al. (2022), for simplicity, we approximate the local photon density at specific radii in the AGN disk with a blackbody spectrum (in the units of $\text{erg}^{-1} \text{cm}^{-3}$),

$$n_d(\varepsilon_{\gamma}) = \frac{8\pi}{(hc)^3} \frac{\varepsilon_{\gamma}^2}{\exp(\varepsilon_{\gamma}/k_B T_{d,\text{eff}})} \quad (2)$$

where ε_{γ} is the photon energy, k_B is the Boltzmann constant, h is Planck constant and c is the speed of light.

2.2. Electron cooling and radiation

Internal dissipation shocks continuously accelerate electrons at the internal dissipation area. In order to get the radiation region electron spectral distribution, we solve the steady-state electron continuity equation,

$$\frac{N'_{\gamma'_e}}{t'_{\text{dyn}}} - \frac{\partial}{\partial \gamma'_e} \left(\dot{\gamma}'_e N'_{\gamma'_e} \right) = \dot{Q}'_{e,\text{inj}} \quad (3)$$

where γ'_e is the electron Lorentz factor, $N'_{\gamma'_e} = dN'_e/d\gamma'_e$ is the spectrum of electron energy, $t'_{\text{dyn}} = r_{\text{diss}}/\Gamma_j c$ is the dynamical timescale of the jet, which can represent adiabatic losses or escape timescale and Γ_j is the jet bulk Lorentz factor. $\dot{\gamma}'_e = \gamma'_e/t'_{e,\text{cool}}$ is the energy loss rate of the electron and $t'_{e,\text{cool}}$ is the cooling timescale of the electron. $\dot{Q}'_{e,\text{inj}}$ is the energy injection rate of the electron, and we consider a power-law distribution with a slope s , e.g., $\dot{Q}'_{e,\text{inj}} \propto (\gamma'_e/\gamma'_{e,m})^{-s}$ (Zhang et al. 2019). Assuming the index $s = 2.2$, the normalization factor for the injection term can be obtained by

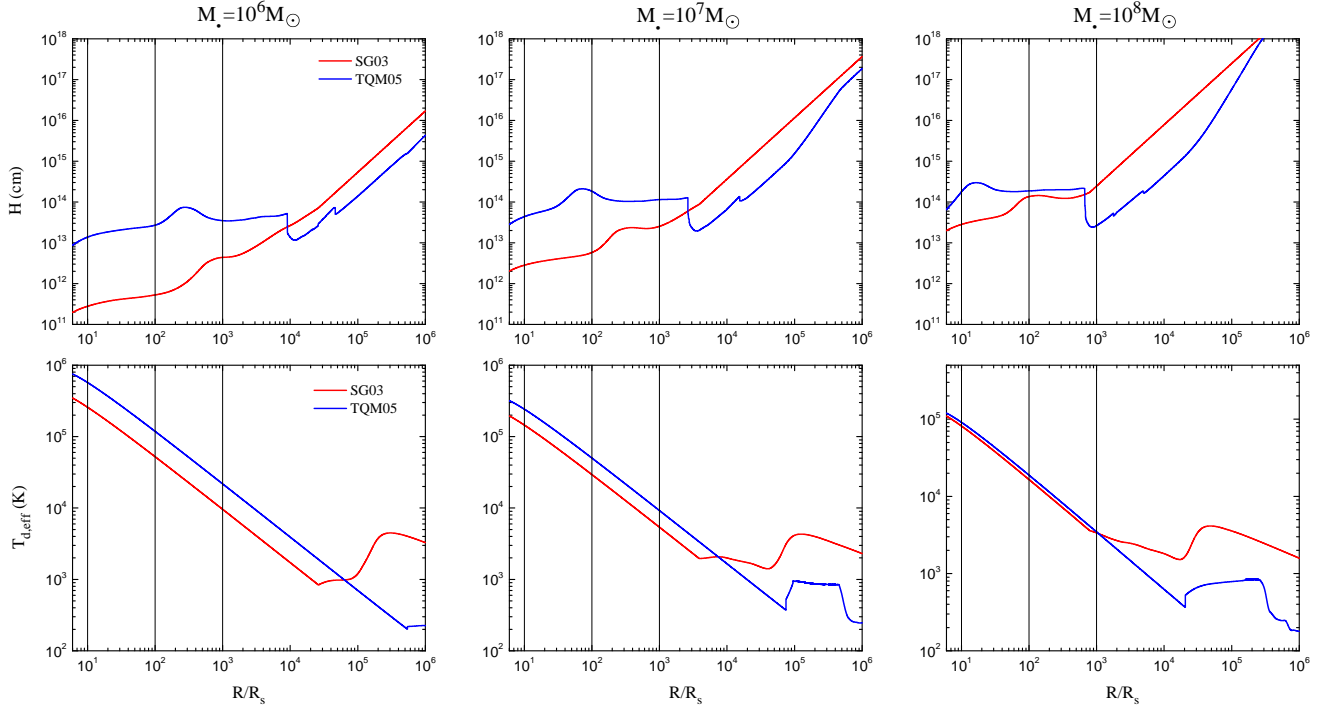


Figure 2. AGN disk profile for the half-thickness H (top row) and effective temperature $T_{\text{d,eff}}$ (bottom row) with $M_{\bullet} = 10^6 M_{\odot}$ (left column), $10^7 M_{\odot}$ (middle column) and $10^8 M_{\odot}$ (right column). The red and blue lines represent the SG03 and TQM05 models, respectively. The vertical lines from left to right in each panel are the distance from the central BH for $10R_s$, $100R_s$, and $1000R_s$, where $R_s = 2GM_{\bullet}/c^2$ is the Schwarzschild radius.

$\int_{\gamma'_{\text{e,m}}}^{\infty} d\gamma'_{\text{e}} \gamma'_{\text{e}} m_{\text{e}} c^2 \dot{Q}'_{\text{e,inj}} = \epsilon_{\text{e}} L_{\text{j,iso}} / \Gamma_{\text{j}}^2$, where m_{e} is the mass of the electron, $L_{\text{j,iso}}$ is the isotropic kinetic luminosity of the jet, ϵ_{e} is the fraction of jet kinetic energy that is converted to electrons and $\gamma'_{\text{e,m}}$ is the minimum Lorentz factor. And we assume $\gamma'_{\text{e,m}} = 100$ (Yuan et al. 2022). Within the internal dissipation region, electrons are accelerated by shocks with an acceleration timescale of $t'_{\text{e,acc}} = \gamma'_{\text{e}} m_{\text{e}} c / e B'$, where e is the electron charge, $B' = \sqrt{2\epsilon_B L_{\text{j,iso}} / r_{\text{diss}}^2 \Gamma_{\text{j}}^2 c}$ is the strength of the magnetic field and ϵ_B is the fraction of jet kinetic energy that is converted to magnetic field.

Accelerated electrons lose energy via different mechanisms (Bošnjak et al. 2009), e.g., synchrotron emissions, inverse Compton (IC) process, and adiabatic cooling. The cooling rate of the electron for these mechanisms can be represented by $\dot{\gamma}'_{\text{e,syn}}$, $\dot{\gamma}'_{\text{e,IC}}$ and $\dot{\gamma}'_{\text{e,adi}}$, which can be expressed as (Jones 1968; Blumenthal & Gould 1970; Fan et al. 2008; Uhm et al. 2012; Geng et al. 2018),

$$\dot{\gamma}'_{\text{e,syn}} = \frac{\sigma_{\text{T}} B'^2 \gamma_{\text{e}}'^2}{6\pi m_{\text{e}} c} \quad (4)$$

$$\dot{\gamma}'_{\text{e,IC}} = \frac{1}{m_{\text{e}} c^2} \frac{3\sigma_{\text{T}}}{4\gamma_{\text{e}}'^2} \int_{\nu'_{\text{min}}}^{\nu'_{\text{max}}} \frac{n'(\nu') d\nu'}{\nu'} \times \int_{\nu'_{\text{IC,min}}}^{\nu'_{\text{IC,max}}} h\nu'_{\text{IC}} d\nu'_{\text{IC}} F(q, g) \quad (5)$$

$$\dot{\gamma}'_{\text{e,adi}} = \gamma'_{\text{e}} / t'_{\text{dyn}} \quad (6)$$

the corresponding cooling timescales are presented by $t'_{\text{e,syn}}$, $t'_{\text{e,IC}}$ and $t'_{\text{e,adi}}$, respectively. σ_{T} is the Thomson cross section. ν' is the frequency and $n'(\nu')$ is the number density of the seed photon for a specific frequency, and there are two different sources of the seed photon, electron synchrotron (n'_{syn}) and AGN disk photon (n'_{d}) fields. And the corresponding inverse Compton processes are presented as synchrotron self-Compton (SSC) and external inverse Compton (EIC), with cooling rates denoted by $\dot{\gamma}'_{\text{e,SSC}}$ and $\dot{\gamma}'_{\text{e,EIC}}$ (the cooling timescale denoted by $t'_{\text{e,SSC}}$ and $t'_{\text{e,EIC}}$), respectively. $F(q, g) = 2q \ln q + (1 + 2q)(1 - q) + \frac{(4qg)^2}{2(1+4qg)}(1 - q)$, where $g = \frac{\gamma'_{\text{e}} h \nu'}{m_{\text{e}} c^2}$, $w = \frac{h \nu'_{\text{IC}}}{\gamma'_{\text{e}} m_{\text{e}} c^2}$ and $q = \frac{w}{4g(1-w)}$. The lower and upper limits of ν'_{IC} are $\nu'_{\text{IC,min}} = \nu'$ and $\nu'_{\text{IC,max}} = \frac{\gamma'_{\text{e}} m_{\text{e}} c^2}{h} \frac{4g}{4g+1}$, respectively. For simplicity, the secondary IC is omitted in our consideration. Therefore,

the total cooling rate of the electron is

$$\dot{\gamma}'_{\text{e,cool}} = \dot{\gamma}'_{\text{e,adi}} + \dot{\gamma}'_{\text{e,syn}} + \dot{\gamma}'_{\text{e,SSC}} + \dot{\gamma}'_{\text{e,EIC}} \quad (7)$$

The synchrotron radiation power for a specific ν' ,

$$P'_{\text{syn}}(\nu') = \frac{\sqrt{3}e^3B'}{m_{\text{e}}c^2} \int_{\gamma'_{\text{e,min}}}^{\gamma'_{\text{e,max}}} N'_{\gamma'_{\text{e}}} F(\nu'/\nu'_{\text{c}}) d\gamma'_{\text{e}} \quad (8)$$

and the number density of synchrotron photons is

$$n'_{\text{syn}}(\nu') = \frac{1}{4\pi r_{\text{diss}}^2} \frac{P'_{\text{syn}}(\nu')}{ch\nu'} \quad (9)$$

where $\nu'_{\text{c}} = 3eB'\gamma_{\text{e}}'^2/(4\pi m_{\text{e}}c)$ is the characteristic frequency, $F(\nu'/\nu'_{\text{c}}) = \nu'/\nu'_{\text{c}} \int_{\nu'_{\text{c}}}^{\infty} K_{5/3}(\xi) d\xi$ and $K_{5/3}(\xi)$ is the modified Bessel function of 5/3 order. The power of IC process can be expressed as (Blumenthal & Gould 1970; Fan et al. 2008),

$$P'_{\text{IC}}(\nu'_{\text{IC}}) = \frac{3\sigma_{\text{T}}ch\nu'_{\text{IC}}}{4} \int_{\nu'_{\text{min}}}^{\nu'_{\text{max}}} \frac{n'(\nu')d\nu'}{\nu'} \times \int_{\gamma'_{\text{e,min}}}^{\gamma'_{\text{e,max}}} \frac{F(q,g)}{\gamma'^2} N'_{\gamma'_{\text{e}}} d\gamma'_{\text{e}} \quad (10)$$

and the photon number density,

$$n'_{\text{IC}}(\nu'_{\text{IC}}) = \frac{1}{4\pi r_{\text{diss}}^2} \frac{P'_{\text{IC}}(\nu'_{\text{IC}})}{ch\nu'_{\text{IC}}} \quad (11)$$

By substituting n'_{syn} and n'_{d} into Eq.11, we obtain the photon number density separately for SSC and EIC processes individually. The jet propagating in the cavity undergoes high-energy photon attenuation due to pair production with low-energy photons from the AGN disk's radiation field (i.e., $\gamma\gamma$ attenuation) when $\varepsilon'\varepsilon'_{\text{seed}} \gtrsim (m_{\text{e}}c^2)^2$, where ε' is the high-energy photons energy and $\varepsilon'_{\text{seed}}$ is the low-energy target photons energy. The $\gamma\gamma$ process optical depth is (Zhang et al. 2021; Murase et al. 2011),

$$\tau_{\gamma\gamma} = H/2 \int_{-1}^1 d\mu (1-\mu) \int d\varepsilon' n'_{\text{d}}(\varepsilon') \sigma_{\gamma\gamma}(S) \quad (12)$$

and

$$\sigma_{\gamma\gamma}(S) = \frac{3}{16} \sigma_{\text{T}} (1 - \beta_{\text{cm}}^2) \times \left[(3 - \beta_{\text{cm}}^4) \ln \frac{1 + \beta_{\text{cm}}}{1 - \beta_{\text{cm}}} - 2\beta_{\text{cm}} (2 - \beta_{\text{cm}}^2) \right]$$

is the annihilation cross section. $\beta_{\text{cm}} = \sqrt{1 - 4/S}$ and $S = 2\varepsilon'\varepsilon'_{\text{seed}}(1 - \mu)$ is the Mandelstam variable.

2.3. protons cooling and neutrino emission

We use $n'_{\gamma}(\varepsilon'_{\gamma})$ to express the photon density in a dissipation region for a specific photon energy ε'_{γ} , which is the seed photons for the $\text{p}\gamma$ process. We adopt the minimum and maximum photon energy as $\varepsilon'_{\gamma,m} = 0.1 \text{ eV}$ and $\varepsilon'_{\gamma,M} = 10^6 \text{ eV}$, respectively, as in Murase & Nagataki (2006). Besides, the specific proton energy distribution can be expressed as

$$n_{\text{p}}(\varepsilon_p) \propto \varepsilon_p^{-2} \quad (13)$$

where ε_p is the proton energy. The total energy of the protons $E_{\text{p,iso}} = \epsilon_{\text{p}} E_{\text{j,iso}}$, where ϵ_{p} is the fraction of jet kinetic energy that is converted to protons, $E_{\text{j,iso}} = L_{\text{j,iso}} t_{\text{j}}$ is the isotropic kinetic and t_{j} is the duration of the jet. The minimum proton energy $\varepsilon_{\text{p,m}} = \Gamma_{\text{j}} \varepsilon'_{\text{p,m}} = \Gamma_{\text{j}} (10m_{\text{p}}c^2)$ and the maximum energy can be obtained by balancing the acceleration and cooling timescale,

$$t'_{\text{p,acc}}^{-1} > t'_{\text{p,cool}}^{-1} = t'_{\text{dyn}}^{-1} + t'_{\text{syn}}^{-1} + t'_{\text{p}\gamma}^{-1} \quad (14)$$

where the acceleration timescale $t'_{\text{p,acc}} = \varepsilon'_{\text{p}}/(ecB')$, the proton synchrotron cooling timescale $t'_{\text{p,syn}} = 6\pi m_{\text{p}}^4 c^3 / (m_{\text{p}}^2 \sigma_{\text{T}} B'^2 \varepsilon_{\text{p}})$ and the photomeson cooling rate (Waxman & Bahcall 1997),

$$t'_{\text{p}\gamma}^{-1} = \frac{c}{2\gamma_{\text{p}}'^2} \int_{\bar{\varepsilon}_{\text{th}}}^{\infty} d\bar{\varepsilon}_{\gamma} \sigma_{\text{p}\gamma} \kappa_{\text{p}\gamma} \bar{\varepsilon}_{\gamma} \int_{\bar{\varepsilon}_{\gamma}/2\gamma_{\text{p}}'}^{\infty} d\varepsilon'_{\gamma} \varepsilon'_{\gamma}^{-2} n'_{\gamma}(\varepsilon'_{\gamma}) \quad (15)$$

where $\gamma_{\text{p}}' = \varepsilon'_{\text{p}}/m_{\text{p}}c^2$ is the Lorentz factor of the proton, $\bar{\varepsilon}_{\gamma}$ is the photon energy in the proton rest frame, and $\bar{\varepsilon}_{\text{th}} \approx 145 \text{ MeV}$ is the threshold energy for the photomeson production. $\sigma_{\text{p}\gamma}$ and $\kappa_{\text{p}\gamma}$ are the cross-section and inelasticity for photomeson production, respectively. We use the fitting formulae based on GEANT4 in Kossow (2002) for $\sigma_{\text{p}\gamma}$. There is not a simply fitting formulae for $\kappa_{\text{p}\gamma}$, so we adopt $\kappa_{\text{p}\gamma} = 0.2$ for $\bar{\varepsilon}_{\gamma} < 983 \text{ MeV}$ and $\kappa_{\text{p}\gamma} = 0.6$ for $\bar{\varepsilon}_{\gamma} > 983 \text{ MeV}$ (Atoyan & Dermer 2001).

Pions produced by the photomeson process decay into a muon and a muon neutrino. The spectrum of the muon neutrino can be expressed as,

$$\varepsilon_{\nu_{\mu}}^2 n_{\nu_{\mu}} \approx 1/8 f_{\text{p}\gamma} f_{\text{sup},\pi} \varepsilon_{\text{p}}^2 n_{\text{p}} \quad (16)$$

where $\varepsilon_{\nu_{\mu}} \approx 0.05 \varepsilon_{\text{p}}$ is the muon neutrino energy, $f_{\text{p}\gamma} = t'_{\text{p,cool}}/t'_{\text{p}\gamma}$ is the fraction of the proton energy into the pions (Kimura et al. 2017) and $f_{\text{sup},\pi} = 1 - \exp(-t_{\pi,\text{cool}}/t_{\pi,\text{dec}})$ is the suppression factor due to the

pions cooling. $t_{\pi,\text{dec}} = \gamma_{\pi}\tau_{\pi}$ is the decay timescale in the frame of pions, $\gamma_{\pi} = \varepsilon_{\pi}/m_{\pi}c^2$ is the Lorentz factor and $\tau_{\pi} = 2.6 \times 10^{-8}$ s. $t_{\pi,\text{cool}}^{-1} = t_{\pi,\text{syn}}^{-1} + t_{\text{dyn}}^{-1}$ is the cooling time and $t_{\pi,\text{syn}}$ is the synchrotron cooling timescale for pions. Pions can decay to electron neutrinos and anti-muon neutrinos with the following energy spectra,

$$\varepsilon_{\nu_e}^2 n_{\nu_e} \approx \varepsilon_{\bar{\nu}_{\mu}}^2 n_{\bar{\nu}_{\mu}} \approx 1/8 f_{p\gamma} f_{\text{sup},\pi} f_{\text{sup},\mu} \varepsilon_p^2 n_p \quad (17)$$

where $\varepsilon_{\nu_e} \approx \varepsilon_{\bar{\nu}_{\mu}} \approx 0.05\varepsilon_p$ are the energy of electron neutrinos and anti-muon neutrinos. $f_{\text{sup},\mu} = 1 - \exp(-t_{\mu,\text{cool}}/t_{\mu,\text{dec}})$ is the suppression factor from muons, where $t_{\mu,\text{dec}} = \gamma_{\mu}\tau_{\mu}$, $\gamma_{\mu} = \varepsilon_{\mu}/m_{\mu}c^2$ is the Lorentz factor of the muons and $\tau_{\mu} = 2.2 \times 10^{-6}$ s. $t_{\mu,\text{cool}}^{-1} = t_{\mu,\text{syn}}^{-1} + t_{\text{dyn}}^{-1}$ is the cooling time and $t_{\mu,\text{syn}}$ is the synchrotron cooling timescale for muons. Besides, neutrino oscillations cause a divergence between the spectrum observed on Earth and the source spectrum, and the fluence can be calculated by (Harrison et al. 2002),

$$\phi_{\nu_e + \bar{\nu}_e} = \frac{10}{18} \phi_{\nu_e + \bar{\nu}_e}^0 + \frac{4}{18} \left(\phi_{\nu_{\mu} + \bar{\nu}_{\mu}}^0 + \phi_{\nu_{\tau} + \bar{\nu}_{\tau}}^0 \right) \quad (18)$$

$$\phi_{\nu_{\mu} + \bar{\nu}_{\mu}} = \frac{4}{18} \phi_{\nu_e + \bar{\nu}_e}^0 + \frac{7}{18} \left(\phi_{\nu_{\mu} + \bar{\nu}_{\mu}}^0 + \phi_{\nu_{\tau} + \bar{\nu}_{\tau}}^0 \right) \quad (19)$$

where $\phi_i^0 = n_i/4\pi d_L^2$ is the neutrino fluence at the source, d_L is the luminosity distance, and ν_{τ} ($\bar{\nu}_{\tau}$) is the tau (anti-tau) neutrino.

3. RESULTS

In this section, we present the specific model parameters in Sec.3.1 and then compute the radiation spectrum for seed photons (Sec.3.2) and neutrinos (Sec.3.3).

3.1. Parameter Setting

We collect the specific parameter values in Table 1, e.g., the properties of the two-component jet, the location of the sGRB within the AGN disk, and the parameters of the AGN disk, where R_{GRB} is the distance of the sGRB from the SMBH in the AGN disk with the unit of $R_s = 2GM_{\bullet}/c^2$. We show the different cases to explore the effect for specific M_{\bullet} and R_{GRB} . Besides, to determine the photon number density of Eq.1, we calculate the peak energy $\varepsilon_{\gamma,p} = \Gamma_j \varepsilon'_{\gamma,p} \approx 900$ keV for the narrow component and 500 keV for the wide component via the relation in Qin & Chen (2013).

3.2. Seed photons for $p\gamma$ processes

Fig. 3 shows the seed photon number density distributions in the jet comoving frame, e.g., Band (Eq.1 dotted lines), EIC (Eq.11, dashed lines), and AGN disk (Eq.2, solid lines) photon fields. The magenta and green lines represent the wide and narrow component jets. In each panel, we use the case in Table 1 for specific M_{\bullet} and R_{GRB} and note it on each panel title.

By analyzing and comparing the results depicted in Fig. 3, we can draw the following conclusions:

- In each case, the EIC photon density is lower than the Band in both narrow and wide components, because EIC upscattering reduces photon density at a specific energy. Therefore, we do not consider the influence of EIC photons in the calculation of neutrino emission.
- The photon number density of the AGN disk photon fields of SG03 (thin green lines) and TQM05 (thick green lines) are much higher than the Band for the narrow component jet in each case. Compared to the SG03 model, the TQM05 model has a higher number density of the AGN disk photon field, which is due to the higher AGN disk temperature of the TQM05 model.
- The narrow jet component has a higher AGN disk photon density than the wide component due to Doppler boosting, attributable to the narrow component with higher Lorentz factor.
- As R_{GRB} (or M_{\bullet}) increases, the number density of the AGN disk photon field gradually decreases in both narrow and wide components, due to the effective temperature of the AGN disk decreasing.

3.3. Neutrino emission

Fig. 4 shows the observable fluence of muon neutrino at $d_L = 300$ Mpc with different seed photon fields. The dotted lines are only the Band photon field for the narrow (green), wide (magenta), and total (black) jet components. Similarly, the thin solid lines are both Band and SG03 photon fields; the thick solid lines are both Band and TQM05 photon fields. Besides, we adopt different M_{\bullet} and R_{GRB} in each panel. Based on the calculation results in Fig. 4, we can draw the following conclusions:

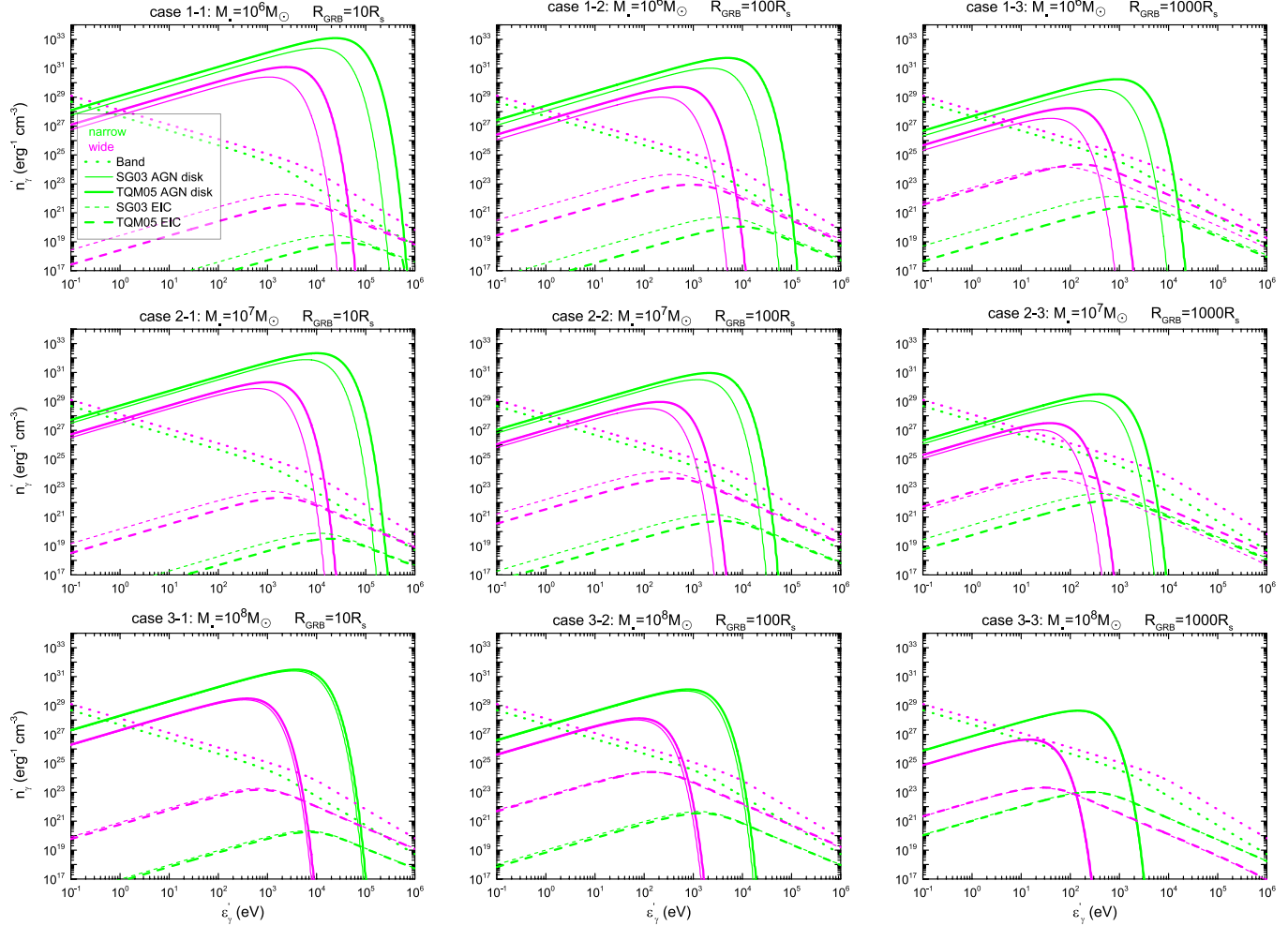


Figure 3. The seed photon number density in the comoving frame for the $p\gamma$ reaction. The green and magenta lines present the number density in the narrow and wide component jets, respectively. The dotted lines are the Band photons for narrow (green) and wide (magenta) components. Similarly, the thin solid lines are the AGN disk photons of SG03, the thick solid lines are the AGN disk photons of TQM05, the thin dashed lines are the EIC of SG03, and the thick dashed lines are the EIC of TQM05. Additionally, each panel title lists the SMBH mass M_\bullet and sGRB location R_{GRB} used in the calculation.

- When solely the Band photons ingredient (dotted black lines) is present in the jet, the energy of neutrinos can range from TeV to EeV. However, When considering both the Band and AGN disk photons (solid black lines), the neutrino energy would be lower, from \sim TeV to \sim PeV (\sim TeV to \sim 10PeV) for $R_{\text{GRB}} \lesssim 100R_s$ (from $R_{\text{GRB}} \lesssim 1000R_s$). Because the AGN disk photon field density can exceed Band, which can suppress the high-energy protons and neutrinos.

- AGN disk photon field can strengthen the neutrino fluence between \sim TeV and \sim PeV, since the higher AGN disk photon field density enhances photomeson production. Besides, the neutrino spectrum

shows a bump (solid black lines) due to sharply increased photomeson efficiency in the narrow and wide components.

- The narrow component dominates neutrino radiation at higher energy, while the wide component concentrates on lower-energy neutrino emissions, due to different Lorentz factors.
- When only the $M_\bullet \lesssim 10^7 M_\odot$, the SG03 (thin solid black lines) and TQM05 (thick solid black lines) models show significant discrepancy.
- As R_{GRB} (or M_\bullet) increases, the influence of the AGN disk photon field becomes weaker, i.e., the

range of neutrino energy would be broader and the peak fluence would be lower (solid black lines).

3.4. Probability of Neutrino Detection

The detectable neutrino counts (N_ν) depend both on the neutrino fluence (ϕ_ν) and the detector effective area (A_{eff}),

$$N_\nu = \int \phi_\nu(\varepsilon_\nu) A_{\text{eff}}(\varepsilon_\nu, \delta) d\varepsilon_\nu \quad (20)$$

where δ is the declination of the neutrino source. We use the effective area of IceCube of a 10-year point source to calculate expected neutrino signal events (IceCube Collaboration et al. 2021). The effective area depends on neutrino energy and declination of the source, which changes at different observational periods due to instrumental variations. We adopt the effective area of IC86II in the calculation. Besides, the effective area of IceCube-Gen2 is ~ 5 times greater than that of IceCube (Aartsen et al. 2021), so we scale IC86II to estimate it. The probability that IceCube detects at least one neutrino can be expressed as (Kimura et al. 2017; Matsui et al. 2023),

$$P(N_\nu \geq 1) = 1 - e^{-N_\nu} \quad (21)$$

For subsequent calculations, we consider the influence of different M_\bullet and R_{GRB} . Besides, we also choose three representative δ intervals to analyze the declination effect, e.g., $-90^\circ \sim -73.74^\circ$, $2.29^\circ \sim 4.59^\circ$ and $73.74^\circ \sim 90^\circ$. The detection probability of IceCube (Gen2) for different cases is shown in Fig. 5. The dotted lines only are the Band photons, and the solid lines consider both the Band and AGN disk photons, where the thin (thick) line is the SG03 (TQM05) model. The black and red lines represent the probability for IceCube and IceCube-Gen2, respectively. We examine three parameters: M_\bullet , R_{GRB} , and δ . We vary δ while maintaining M_\bullet , R_{GRB} constant in each row. And the following conclusions can be drawn,

- Significant differences between the TQM05 and SG03 models appear only in panel (a) for $M_\bullet = 10^6 M_\odot$, $R_{\text{GRB}} = 10R_s$ and $\delta : -90^\circ \sim -73.74^\circ$, e.g., the $d_{\text{L,M}} \approx 1(3)$ Mpc for IceCube(Gen2) with the TQM05 model and $d_{\text{L,M}} \approx 5(10)$ Mpc for IceCube(Gen2) with the SG03 model, where $d_{\text{L,M}}$ is the largest d_{L} for $P \sim 1$.
- When $\delta : -90^\circ \sim -73.74^\circ$ and $R_{\text{GRB}} \lesssim 10R_s$ for $M_\bullet = 10^6 M_\odot$, $d_{\text{L,M}}$ of only Band photons (black

dotted lines) is larger than both Band+TQM05 (solid thick black lines) and Band+SG03 (solid thin black lines) for IceCube. While in other cases (panel b-i), only Band photons is smaller than both Band+TQM05 and Band+SG03 for IceCube.

- In panel (a), the $d_{\text{L,M}}$ of Band+SG03 (Band+TQM05) is much less than only Band, since the neutrino emissions concentrate on $\varepsilon_\nu < 10^5$ GeV, but the effective area of IceCube is much smaller at this energy range.
- When M_\bullet and R_{GRB} are fixed (comparing in each row), $d_{\text{L,M}}$ would increase with δ for Band+SG03 and Band+TQM05, which is due to IceCube's effective area being larger in the lower energy. Similarly, only increasing M_\bullet (R_{GRB}), $d_{\text{L,M}}$ also can increase, due to more neutrino fluence.
- Only containing Band photons, the $d_{\text{L,M}}$ of IceCube (Gen2) can reach 50 (100) Mpc. Under the influence of AGN disk photons, the $d_{\text{L,M}}$ of IceCube (Gen2) can reach 100 (200) Mpc, e.g., panels b, c, and i.

4. CONCLUSIONS AND DISCUSSIONS

BCOs (BNS, NS-BH) developing in AGN disks can create a low-density cavity through hydrodynamic interactions, with dimensions comparable to the AGN disk height. BCOs merger can produce a relativistic GRB jet. As the jet propagates within the cavity, the motion of the jet is not affected by the matter of the AGN disk, but the photon field of the AGN disk will alter the radiation of the internal dissipation region. The seed photon fields within the jet internal dissipation region consist of three ingredients, i.e., Band, EIC, and AGN disk photon fields. Our research employs a structured jet (e.g., two-component) flowing orthogonally to the mid-plane of the AGN disk. Based on these assumptions, we calculate the seed photon and the neutrino emission from the jet within the internal dissipation region by considering the potentially effect of different AGN disk models (e.g., SG03 and TQM05). Our research can conclude as,

1. The photon density of EIC is lower than Band in the narrow and wide jet components for each case in Table 1.

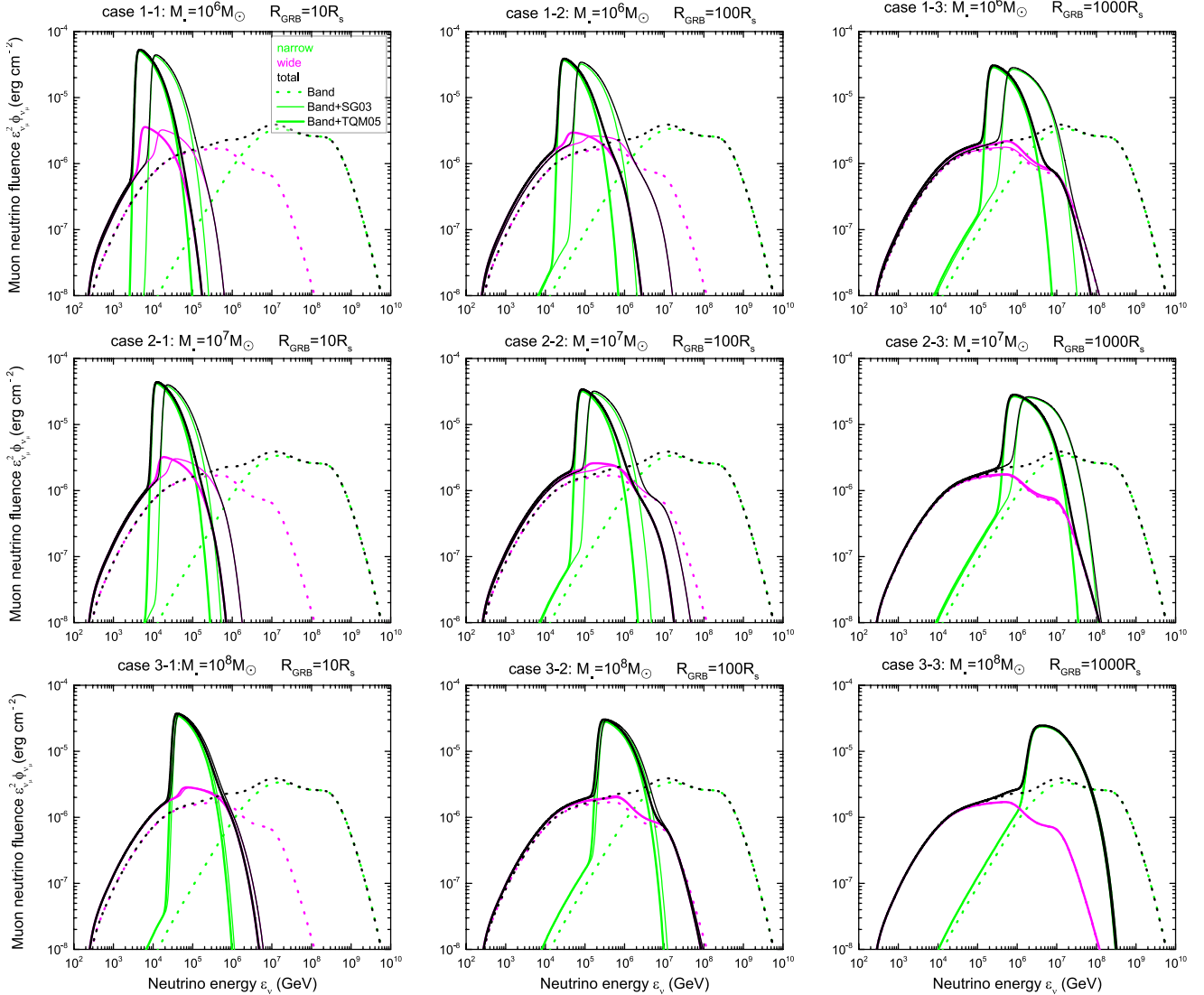


Figure 4. The observable fluence of muon neutrino at $d_L = 300$ Mpc with different seed photon sources. The green, magenta, and black lines are the contributions of the narrow, wide and total components, respectively. Similarly, the dotted lines are the only Band photons ingredient, the thin solid lines are the Band and SG03 AGN disk photons ingredients and the thick solid lines are the Band and TQM05 AGN disk photons ingredients.

2. Only when $M_* \lesssim 10^7 M_\odot$, the SG03 and TQM05 models can exhibit large differences.
3. The AGN disk photon density is higher than the Band in the narrow component, which can significantly affect the neutrino emission. The AGN disk photon number density would be lower than Band for large M_* and R_{GRB} .
4. The narrow component dominates neutrino radiation at higher energies, while the wide component concentrates on lower-energy neutrino emissions. Compared to the top-hat jet, the two-component

jet can generate neutrino radiation with a broader energy range and form two bumps in the neutrino fluence.

5. Compared with only the Band, the AGN disk photon field significantly affects the neutrino radiation of the jet, which can suppress high-energy neutrinos from \sim PeV to \sim EeV and significantly enhance the fluence from \sim TeV to \sim PeV.
6. Considering the impact of the AGN disk photon field, the $d_{L,M}$ of IceCube (Gen2) can reach 100

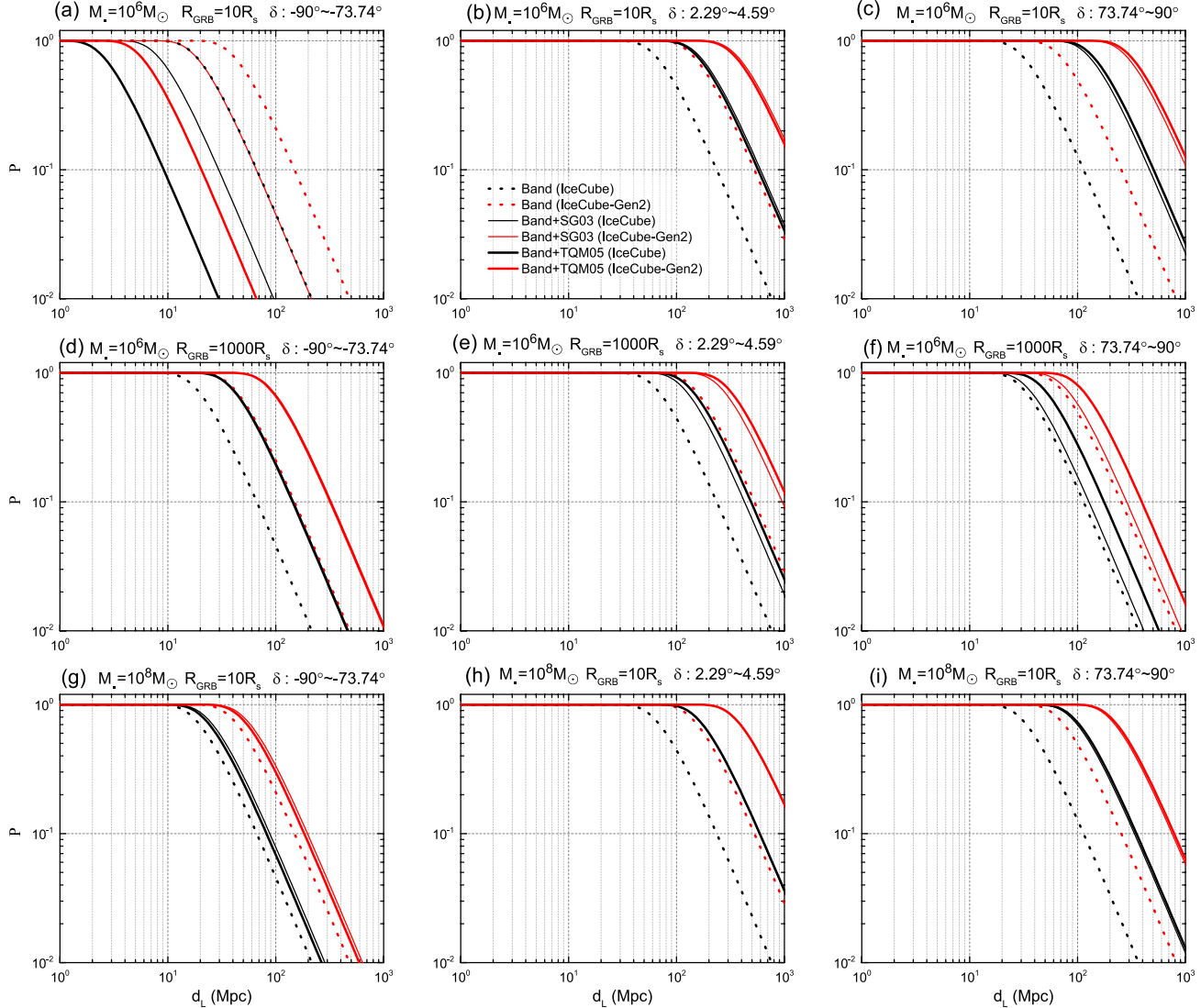


Figure 5. The probability of neutrino detection. The dotted lines only contain the influence of Band photons, and the solid lines consider both the Band and AGN disk photons (thin: SG03, thick: TQM05). The black and red lines represent the probability for IceCube and Gen2, respectively. In the up (middle, or bottom) row, we fix $M_* = 10^6 M_\odot$, $R_{\text{GRB}} = 10 R_s$ ($M_* = 10^6 M_\odot$, $R_{\text{GRB}} = 1000 R_s$, or $M_* = 10^8 M_\odot$, $R_{\text{GRB}} = 10 R_s$) and change δ in each panel.

(200) Mpc, which is roughly twice that of only Band photons.

Taking into account the influence of the AGN disk photon field, the neutrino radiation is concentrated in the energy range from TeV to PeV. We anticipate that the new-generation neutrino detectors will possess higher sensitivity and larger effective areas to search for the neutrino radiation generated by sGRB jets in the AGN disk and validate our model, e.g., Baikal-GVD (Avrorin et al. 2011), IceCube-Gen2 and KM3NeT (Adrián-Martínez et al. 2016). Besides, searching for neutrinos from sGRB jets in AGN disks can help ana-

lyze jet composition and the central engine (Ou et al. 2024).

The sGRBs in the AGN disk are ideal sources for multi-messenger observations. Except for neutrino and EM emission from the jet in the research, before the BCO merger, the wind generated by accretion interacts with the material in the AGN disk to produce EM and neutrino radiation (Wang et al. 2021; Kimura et al. 2021; Zhou et al. 2023). Furthermore, the evolution of a single compact star within the AGN disk can also generate the wind and accompanying radiation (Chen et al. 2023). GW observations will be crucial for determining

Table 1. Model parameters setting

| | | Two component jet | | | |
|------------------------------|--|-------------------|--------------------|-----------|--|
| | | narrow | wide | | |
| Γ_j | | 300 | | 30 | |
| $L_{j,iso}$ (erg s $^{-1}$) | | 10^{53} | | 10^{52} | |
| t_j (s) | | | 1 | | |
| s | | | 2.2 | | |
| ϵ_e | | | 0.1 | | |
| ϵ_B | | | 0.01 | | |
| ϵ_p | | | 0.3 | | |
| r_{diss} (cm) | | | 5×10^{13} | | |

| GRB positions and AGN disk | | | | | |
|----------------------------|---------------------|---------------|-----------------------|-----------------------|--------------------|
| | M_\bullet/M_\odot | R_{GRB}/R_s | H (cm) | $T_{d,eff}$ (K) | |
| | | | SG model | TQM model | SG model |
| case 1-1 | 10^6 | 10 | 2.79×10^{11} | 1.38×10^{13} | 2.58×10^5 |
| case 1-2 | | 100 | 5.27×10^{11} | 2.71×10^{13} | 5.23×10^4 |
| case 1-3 | | 1000 | 4.39×10^{12} | 3.48×10^{13} | 9.58×10^3 |
| case 2-1 | 10^7 | 10 | 2.83×10^{12} | 4.38×10^{13} | 1.45×10^5 |
| case 2-2 | | 100 | 5.78×10^{12} | 1.84×10^{14} | 2.94×10^4 |
| case 2-3 | | 1000 | 2.53×10^{13} | 1.15×10^{14} | 5.39×10^3 |
| case 3-1 | 10^8 | 10 | 2.82×10^{13} | 1.77×10^{14} | 8.16×10^4 |
| case 3-2 | | 100 | 1.36×10^{14} | 1.87×10^{14} | 1.65×10^4 |
| case 3-3 | | 1000 | 2.45×10^{14} | 2.63×10^{13} | 3.37×10^3 |

the EM and neutrino radiation from the pre- or post-merger. Therefore, we expect the next generation of space-based GW detectors can capture the GW signal within the BCO inspire, e.g., Laser Interferometer Space Antenna (LISA, Amaro-Seoane et al. 2017) and TianQin (Luo et al. 2016).

¹ We are very grateful to Chichuan Jin for helpful discussions. This work is supported by the National Natural Science Foundation of China under grants 12473012 and 12533005, and the National Key R&D Program of China (No. 2023YFC2205901). W.H.Lei. acknowledges support by the science research grants from the China Manned Space Project with NO.CMS-CSST-2021-B11.

REFERENCES

Aartsen, M. G., Abbasi, R., Ackermann, M., et al. 2021, Journal of Physics G Nuclear Physics, 48, 060501, doi: [10.1088/1361-6471/abbd48](https://doi.org/10.1088/1361-6471/abbd48)

Abbott, B. P., Abbott, R., Abbott, T. D., et al. 2017, PhRvL, 119, 161101, doi: [10.1103/PhysRevLett.119.161101](https://doi.org/10.1103/PhysRevLett.119.161101)

Abbott, R., Abbott, T. D., Abraham, S., et al. 2020, PhRvL, 125, 101102, doi: [10.1103/PhysRevLett.125.101102](https://doi.org/10.1103/PhysRevLett.125.101102)

Adrián-Martínez, S., Ageron, M., Aharonian, F., et al. 2016, Journal of Physics G Nuclear Physics, 43, 084001, doi: [10.1088/0954-3899/43/8/084001](https://doi.org/10.1088/0954-3899/43/8/084001)

Amaro-Seoane, P., Audley, H., Babak, S., et al. 2017, arXiv e-prints, arXiv:1702.00786, doi: [10.48550/arXiv.1702.00786](https://doi.org/10.48550/arXiv.1702.00786)

Atoyan, A., & Dermer, C. D. 2001, PhRvL, 87, 221102, doi: [10.1103/PhysRevLett.87.221102](https://doi.org/10.1103/PhysRevLett.87.221102)

Avrorin, A., Aynutdinov, V., Belolaptikov, I., et al. 2011, Nuclear Instruments and Methods in Physics Research A, 639, 30, doi: [10.1016/j.nima.2010.09.137](https://doi.org/10.1016/j.nima.2010.09.137)

Band, D., Matteson, J., Ford, L., et al. 1993, ApJ, 413, 281, doi: [10.1086/172995](https://doi.org/10.1086/172995)

Blumenthal, G. R., & Gould, R. J. 1970, Reviews of Modern Physics, 42, 237, doi: [10.1103/RevModPhys.42.237](https://doi.org/10.1103/RevModPhys.42.237)

Bošnjak, Ž., Daigne, F., & Dubus, G. 2009, *A&A*, 498, 677, doi: [10.1051/0004-6361/200811375](https://doi.org/10.1051/0004-6361/200811375)

Chen, K., Ren, J., & Dai, Z.-G. 2023, *ApJ*, 948, 136, doi: [10.3847/1538-4357/acc45f](https://doi.org/10.3847/1538-4357/acc45f)

Dai, Z. G., & Gou, L. J. 2001, *ApJ*, 552, 72, doi: [10.1086/320463](https://doi.org/10.1086/320463)

Fan, Y.-Z., Piran, T., Narayan, R., & Wei, D.-M. 2008, *MNRAS*, 384, 1483, doi: [10.1111/j.1365-2966.2007.12765.x](https://doi.org/10.1111/j.1365-2966.2007.12765.x)

Gangardt, D., Trani, A. A., Bonnerot, C., & Gerosa, D. 2024, *MNRAS*, 530, 3689, doi: [10.1093/mnras/stae1117](https://doi.org/10.1093/mnras/stae1117)

Geng, J.-J., Huang, Y.-F., Wu, X.-F., Zhang, B., & Zong, H.-S. 2018, *ApJS*, 234, 3, doi: [10.3847/1538-4365/aa9e84](https://doi.org/10.3847/1538-4365/aa9e84)

Goldstein, A., Veres, P., Burns, E., et al. 2017, *ApJL*, 848, L14, doi: [10.3847/2041-8213/aa8f41](https://doi.org/10.3847/2041-8213/aa8f41)

Graham, M. J., Ford, K. E. S., McKernan, B., et al. 2020, *PhRvL*, 124, 251102, doi: [10.1103/PhysRevLett.124.251102](https://doi.org/10.1103/PhysRevLett.124.251102)

Graham, M. J., McKernan, B., Ford, K. E. S., et al. 2023, *ApJ*, 942, 99, doi: [10.3847/1538-4357/aca480](https://doi.org/10.3847/1538-4357/aca480)

Harrison, P. F., Perkins, D. H., & Scott, W. G. 2002, *Physics Letters B*, 530, 167, doi: [10.1016/S0370-2693\(02\)01336-9](https://doi.org/10.1016/S0370-2693(02)01336-9)

IceCube Collaboration, Abbasi, R., Ackermann, M., et al. 2021, arXiv e-prints, arXiv:2101.09836, doi: [10.48550/arXiv.2101.09836](https://doi.org/10.48550/arXiv.2101.09836)

Jin, Z. P., Yan, T., Fan, Y. Z., & Wei, D. M. 2007, *ApJL*, 656, L57, doi: [10.1086/512971](https://doi.org/10.1086/512971)

Jones, F. C. 1968, *Physical Review*, 167, 1159, doi: [10.1103/PhysRev.167.1159](https://doi.org/10.1103/PhysRev.167.1159)

Kimura, S. S., Murase, K., & Bartos, I. 2021, *ApJ*, 916, 111, doi: [10.3847/1538-4357/ac0535](https://doi.org/10.3847/1538-4357/ac0535)

Kimura, S. S., Murase, K., Mészáros, P., & Kiuchi, K. 2017, *ApJL*, 848, L4, doi: [10.3847/2041-8213/aa8d14](https://doi.org/10.3847/2041-8213/aa8d14)

Kossov, M. V. 2002, *European Physical Journal A*, 14, 377, doi: [10.1140/epja/i2002-10008-x](https://doi.org/10.1140/epja/i2002-10008-x)

Luo, J., Chen, L.-S., Duan, H.-Z., et al. 2016, *Classical and Quantum Gravity*, 33, 035010, doi: [10.1088/0264-9381/33/3/035010](https://doi.org/10.1088/0264-9381/33/3/035010)

Lynden-Bell, D. 1969, *Nature*, 223, 690, doi: [10.1038/223690a0](https://doi.org/10.1038/223690a0)

Ma, Z.-P., & Wang, K. 2024, *ApJ*, 970, 127, doi: [10.3847/1538-4357/ad5678](https://doi.org/10.3847/1538-4357/ad5678)

Ma, Z.-P., Wang, K., Zuo, Y.-Y., Zou, Y.-C., & Huang, Y.-H. 2025, arXiv e-prints, arXiv:2511.06707, doi: [10.48550/arXiv.2511.06707](https://doi.org/10.48550/arXiv.2511.06707)

Matsui, R., Kimura, S. S., Toma, K., & Murase, K. 2023, *ApJ*, 950, 190, doi: [10.3847/1538-4357/acd004](https://doi.org/10.3847/1538-4357/acd004)

McKinney, J. C., & Uzdensky, D. A. 2012, *MNRAS*, 419, 573, doi: [10.1111/j.1365-2966.2011.19721.x](https://doi.org/10.1111/j.1365-2966.2011.19721.x)

Mészáros, P., & Rees, M. J. 2000, *ApJ*, 530, 292, doi: [10.1086/308371](https://doi.org/10.1086/308371)

Murase, K., Guetta, D., & Ahlers, M. 2016, *Phys. Rev. Lett.*, 116, 071101, doi: [10.1103/PhysRevLett.116.071101](https://doi.org/10.1103/PhysRevLett.116.071101)

Murase, K., & Nagataki, S. 2006, *PhRvL*, 97, 051101, doi: [10.1103/PhysRevLett.97.051101](https://doi.org/10.1103/PhysRevLett.97.051101)

Murase, K., Toma, K., Yamazaki, R., & Mészáros, P. 2011, *ApJ*, 732, 77, doi: [10.1088/0004-637X/732/2/77](https://doi.org/10.1088/0004-637X/732/2/77)

Ou, Y.-D.-J., Lü, H.-J., Chang, X.-Z., Liu, X.-X., & Liang, E.-W. 2024, *ApJ*, 976, 174, doi: [10.3847/1538-4357/ad8635](https://doi.org/10.3847/1538-4357/ad8635)

Preece, R. D., Briggs, M. S., Mallozzi, R. S., et al. 1998, *ApJL*, 506, L23, doi: [10.1086/311644](https://doi.org/10.1086/311644)

—. 2000, *ApJS*, 126, 19, doi: [10.1086/313289](https://doi.org/10.1086/313289)

Qin, Y.-P., & Chen, Z.-F. 2013, *MNRAS*, 430, 163, doi: [10.1093/mnras/sts547](https://doi.org/10.1093/mnras/sts547)

Rees, M. J., & Meszaros, P. 1994, *ApJL*, 430, L93, doi: [10.1086/187446](https://doi.org/10.1086/187446)

Savchenko, V., Ferrigno, C., Kuulkers, E., et al. 2017, *ApJL*, 848, L15, doi: [10.3847/2041-8213/aa8f94](https://doi.org/10.3847/2041-8213/aa8f94)

Shakura, N. I., & Sunyaev, R. A. 1973, *A&A*, 24, 337

Sirko, E., & Goodman, J. 2003, *MNRAS*, 341, 501, doi: [10.1046/j.1365-8711.2003.06431.x](https://doi.org/10.1046/j.1365-8711.2003.06431.x)

Thompson, T. A., Quataert, E., & Murray, N. 2005, *ApJ*, 630, 167, doi: [10.1086/431923](https://doi.org/10.1086/431923)

Uhm, Z. L., Zhang, B., Hascoët, R., et al. 2012, *ApJ*, 761, 147, doi: [10.1088/0004-637X/761/2/147](https://doi.org/10.1088/0004-637X/761/2/147)

Wang, J.-M., Liu, J.-R., Ho, L. C., Li, Y.-R., & Du, P. 2021, *ApJL*, 916, L17, doi: [10.3847/2041-8213/ac0b46](https://doi.org/10.3847/2041-8213/ac0b46)

Waxman, E., & Bahcall, J. 1997, *PhRvL*, 78, 2292, doi: [10.1103/PhysRevLett.78.2292](https://doi.org/10.1103/PhysRevLett.78.2292)

Yuan, C., Murase, K., Guetta, D., et al. 2022, *ApJ*, 932, 80, doi: [10.3847/1538-4357/ac6ddf](https://doi.org/10.3847/1538-4357/ac6ddf)

Yuan, H.-Y., & Lei, W.-H. 2025, *ApJ*, 987, 167, doi: [10.3847/1538-4357/addbe4](https://doi.org/10.3847/1538-4357/addbe4)

Zhang, B. 2018, *The Physics of Gamma-Ray Bursts*, doi: [10.1017/978139226530](https://doi.org/10.1017/978139226530)

Zhang, B. B., Zhang, B., Sun, H., et al. 2018, *Nature Communications*, 9, 447, doi: [10.1038/s41467-018-02847-3](https://doi.org/10.1038/s41467-018-02847-3)

Zhang, B. T., Murase, K., Veres, P., & Mészáros, P. 2021, *ApJ*, 920, 55, doi: [10.3847/1538-4357/ac0cfc](https://doi.org/10.3847/1538-4357/ac0cfc)

Zhang, W., Woosley, S. E., & Heger, A. 2004, *ApJ*, 608, 365, doi: [10.1086/386300](https://doi.org/10.1086/386300)

Zhang, Y., Geng, J.-J., & Huang, Y.-F. 2019, *ApJ*, 877, 89, doi: [10.3847/1538-4357/ab1b10](https://doi.org/10.3847/1538-4357/ab1b10)

Zheng, J.-H., Wang, X.-Y., Liu, R.-Y., & Zhang, B. 2024, *ApJ*, 966, 141, doi: [10.3847/1538-4357/ad3949](https://doi.org/10.3847/1538-4357/ad3949)

Zhou, Z.-H., & Wang, K. 2023, *ApJL*, 958, L12, doi: [10.3847/2041-8213/ad096f](https://doi.org/10.3847/2041-8213/ad096f)

Zhou, Z.-H., Zhu, J.-P., & Wang, K. 2023, ApJ, 951, 74,
doi: [10.3847/1538-4357/acd380](https://doi.org/10.3847/1538-4357/acd380)
Zhu, J.-P., Wang, K., & Zhang, B. 2021a, ApJL, 917, L28,
doi: [10.3847/2041-8213/ac1a17](https://doi.org/10.3847/2041-8213/ac1a17)

Zhu, J.-P., Wang, K., Zhang, B., et al. 2021b, ApJL, 911,
L19, doi: [10.3847/2041-8213/abf2c3](https://doi.org/10.3847/2041-8213/abf2c3)